

Monte Carlo simulation of magnetic behavior of a spin-chain system on a triangular lattice

Xiaoyan Yao, Shuai Dong, Hao Yu, and Junming Liu*

Laboratory of Solid State Microstructures, Nanjing University, Nanjing 210093, China

and International Center for Materials Physics, Chinese Academy of Sciences, Shenyang, China

(Received 16 July 2006; revised manuscript received 26 August 2006; published 23 October 2006)

The magnetization behavior and spin configurations of anisotropic triangular spin-chain systems are investigated using Monte Carlo simulations based on two- and three-dimensional Ising models, in order to understand the fascinating magnetic phenomena observed in $\text{Ca}_3\text{Co}_2\text{O}_6$ compound. By taking into account the strong intrachain ferromagnetic interaction and relatively weak interchain antiferromagnetic interaction, the simulations reproduce quantitatively the temperature-dependent magnetization behaviors against external magnetic field at low temperature. We present the one-to-one correspondence between the magnetizations and the nearest-neighboring pattern-count/spin snapshots, and demonstrate that the steplike magnetizations are ascribed to the inhomogeneous in-plane spin configurations and ferrimagnetically ordered equilibrium state. It is indicated that for the multistep magnetizations that appeared at low temperature, the substeps are always equidistant and the interval of critical magnetic field for spin flip keeps on 1.2 T. However, the inhomogeneity of the spin configurations makes a mean field approach to the magnetization behavior unsuccessful in predicting the multistep magnetizations.

DOI: 10.1103/PhysRevB.74.134421

PACS number(s): 75.30.Kz, 75.60.-d, 75.40.Mg

I. INTRODUCTION

The investigation of low dimensional systems has been an important field of physics for a long time. Low dimensional spin systems such as interactive spin-chains have revealed very interesting magnetic and electronic transport properties, being of great interest for both theoretical and experimental activities.¹⁻³ On the other hand, geometrically frustrated spin systems also have attracted attention in recent years, because competing interactions in these systems produce high degeneracy of states due to spin frustration, and consequently the peculiar magnetic phenomena such as hysteresis and field-dependent magnetizations are often displayed by these systems.⁴ Spin glasses represent one class of these frustrated spin systems.⁵ Nevertheless, it has been discovered that some complicated magnetic compounds exhibit both the low-dimensional structure and frustrated spin configurations, thus offering some special features of application potentials and fundamental significance. As an extraordinary example, CsCoX_3 compounds (X is Cl or Br) have been studied for a long time.⁶ In parallel to experimental activities, the one-dimensional (1D) spin chains arranged on triangular lattice offer a wonderful checkerboard for both theorists and experimentalists to investigate a variety of phenomena induced by low dimensionality and geometrical frustration.

Besides CsCoX_3 compounds mentioned above, another family of 1D spin-chain compounds with general formula $A'_3\text{ABO}_6$ (A' is Ca or Sr, while A and B are transition metal elements) fall into this category.⁷⁻¹⁰ Such compounds are composed of parallel 1D ABO_6 chains aligned along the hexagonal c axis, separated by A'^{2+} ions.¹¹ Each chain is surrounded by six equally spaced chains, forming a two-dimensional (2D) triangular (hexagonal) lattice in the ab plane. Generally, the interchain distance is about double of the intrachain A - B distance, which ensures that the intrachain interaction is much stronger than the interchain one, offering remarkable anisotropy both in structure and physical prop-

erty. As a member of this family, $\text{Ca}_3\text{Co}_2\text{O}_6$ represents one of the most frequently studied compounds due to its complex magnetic properties.¹⁰⁻²⁷ In contrast to the spin-chain CsCoX_3 that exhibits antiferromagnetic (AFM) interaction both along the chains and between the chains,⁶ the intrachain coupling (along c axis) in $\text{Ca}_3\text{Co}_2\text{O}_6$ is ferromagnetic (FM) and the interchain coupling is AFM and much weaker than the intrachain interaction.¹² The very strong anisotropy of the spin interaction in this compound is repeatedly confirmed both experimentally^{13,14,24} and theoretically.²⁵

One of the most fascinating features observed in $\text{Ca}_3\text{Co}_2\text{O}_6$ is a steplike magnetization (M) plotted against magnetic field (h) applied along the chains, i.e., the c axis,^{13,15,23} once temperature T is below some critical value. For details, as T falls down into between 10 K–25 K, M as a function of h increases rapidly with increasing h from $h=0$, and reaches $M_0/3$ (where M_0 is saturated magnetization) at a small h ($h \sim 0.5$ T). Upon further increasing of h , M remains unchanged and the M - h relation exhibits a $M_0/3$ plateau until $h \sim h_c \approx 3.6$ T, above which M jumps up to the saturated value M_0 . More interesting is that at $T < 10$ K, the $M_0/3$ plateau decomposes into three nonzero and equidistant substeps separated at $h_{S1} \approx 1.2$ T and $h_{S2} \approx 2.4$ T below $h_c \approx 3.6$ T, i.e., each step is 1.2 T wide.^{13,15,23}

To understand this peculiar magnetic behavior, much effort has been made on the spin configuration of spin-chain triangular lattice in order to understand the structural origin.^{12,15,26} Although neutron powder diffraction¹² revealed that the wide $M_0/3$ plateau below $h_c \approx 3.6$ T observed at $T \sim 10$ K is attributed to the ferrimagnetic scenario, the origin of the multistep behaviors at low T remains controversial. Three explanations can be highlighted from literature: (i) magnetic field induced transitions between different spin configurations for the chains in the triangular lattice;^{15,25} (ii) quantum tunneling of spin moment among various energy minimal states;²⁴ and (iii) a combination of two relaxation processes: T -independent relaxation and thermally activated

relaxation.²³ Recently, Kudasov²⁶ started from the 2D Ising model and developed an analytical approach to the steplike $M(h)$ behaviors at $T=0$. The equidistant steps of $M(h)$ curve were qualitatively reproduced in his investigation. The present authors started from the same model and performed Monte Carlo (MC) simulation on the field dependence of the magnetization in antiferromagnetically correlated triangular lattice, assuming that each chain is viewed as an effective spin of giant moment.²⁸ The preliminary simulations indicated that the multistep behaviors can be reproduced in a quantitative sense. In that work, it was argued that the magnetic inhomogeneity and the competition between interchain AFM interaction and external field h may be responsible for these peculiar behaviors.

In this paper, we perform extensive simulation on the 2D Ising model in triangular lattice and extend the simulation to the three-dimensional (3D) Ising model, in order to comprehend the anisotropic magnetic property of $\text{Ca}_3\text{Co}_2\text{O}_6$ compound and understand quantitatively the multistep behaviors by investigating the possible spin configurations and inhomogeneous local spin-ordered states under different field h . Besides the influences of the random exchange term, the hysteresis behavior and the effect of next-nearest neighboring interaction are discussed in this paper. The 3D simulation is performed to defend our argument that at low T the intrachain FM interaction is indeed strong, referring to the interchain AFM one, and consequently, each spin chain can be viewed as a giant spin in the 2D simulation. We also propose a mean-field approximation (MFA) to study the magnetic behaviors. It will be shown that the MFA successfully predicts the $M_0/3$ plateau observed at relatively high T although it fails in predicting the multistep behaviors at low T .

The remainder of this paper is organized as follows. In Sec. II the magnetic behavior of the 2D Ising-like model in triangular lattice is investigated by Monte Carlo simulation. In Sec. III we present the Monte Carlo simulation on 3D triangular Ising-like model. Section IV is attributed to the mean-field approximation of the 2D triangular Ising-like model. The conclusion is presented in Sec. V.

II. MONTE CARLO SIMULATION ON 2D ISING MODEL

A. 2D Ising model

For spin-chain compound $\text{Ca}_3\text{Co}_2\text{O}_6$, the 1D spin-chains align along the c axis and form a triangular lattice in the ab plane. The intrachain FM interaction is much stronger than the interchain AFM coupling, indicating strong Ising-like anisotropy in this compound. Based on these structure characters and previous investigations,^{14,15,26} as an approximation each single spin chain can be regarded as a rigid giant spin and the 3D compound may be viewed as a 2D triangular lattice and the resultant magnetic structure should have two-dimensional character. This approximation will be further discussed in Sec. III. Therefore, a 2D Ising-like triangular lattice composed of these rigid giant spins is considered to study the magnetic behavior resulting from the AFM interchain interaction by Monte Carlo simulation.²⁸ Between each nearest-neighboring spin-chain pair only AFM coupling J ($J < 0$) is considered. In addition, considering the spatial

TABLE I. System parameters chosen for the simulation.

Parameter	Value	Parameter	Value
$J(J)$	-3.592×10^{-25}	S^e	32
g	2	A	0.15
$J_{intra}(J)$	8.2842×10^{-23}	$J_{inter}(J)$	-5.5228×10^{-24}

fluctuation of the system and without losing generality, a random exchange interaction term $\Delta_{m,n}$ is taken into account. The Hamiltonian can be written as

$$H = - \sum_{[m,n]} (J + J\Delta_{m,n}) S_m^e S_n^e - h \mu_B g \sum_m S_m^e, \quad (1)$$

$$\Delta_{m,n} = A \cdot R_{m,n}, \quad (2)$$

where S_m^e is the effective spin moment of a spin chain with the value $\pm S^e$; h is the magnetic field applied along the direction of up-spin chains ($+c$ axis); g is the Lande factor and μ_B is the Bohr magneton; $[m,n]$ denotes the summation over all the nearest-neighboring pairs; $R_{m,n}$ is the random number in $[-1, 1]$, and parameter A represents the magnitude of random exchange interaction. Here it should be noted that S^e and J have different values in different materials, and the real values of the two parameters are not available from experiments. So in our simulation the reasonable values of them are determined by a quantitative comparison between the simulated results and experimental data, which had been discussed in Ref. 28. The values of these parameters for the simulation are shown in Table I.

The Monte Carlo simulation is performed in an $L \times L$ ($L = 100$) Ising-like triangular lattice with periodic boundary conditions. For an arbitrarily chosen initial state, the standard Metropolis algorithm is employed to reach the equilibrium, namely the evolution of the system has reached a stationary state and the energy of the system does not change with Monte Carlo sequence. Considering the fluctuation of evaluated lattice energy, our criterion of equilibrium is that the fluctuation of the lattice average energy within 20 000 MC steps is $\sim 1\%$. Based on the spin configuration the magnetization M is evaluated. The next state is calculated starting from the spin configuration of the previous state. Considering the steady-static hysteretic effect, we evaluate two types of $M(h)$ curves, i.e., the $M(h)$ curves marking FD are calculated upon h decreasing while the others are upon h increasing.

B. Stepwise behavior of magnetization

The simulated M (normalized by the saturated magnetization M_0) as a function of T under different h are shown in Fig. 1(a). It is clearly seen that M as a function of T over the whole T range is strongly h dependent. The change of M with T can be partitioned into three regimes, namely high T range (H), intermediate T range (I), and low T range (L), though the boundaries between them are relatively faint. The simulated M as a function of h shows different behaviors in the three T regimes. In regime H ($T > \sim 35$ K), the response

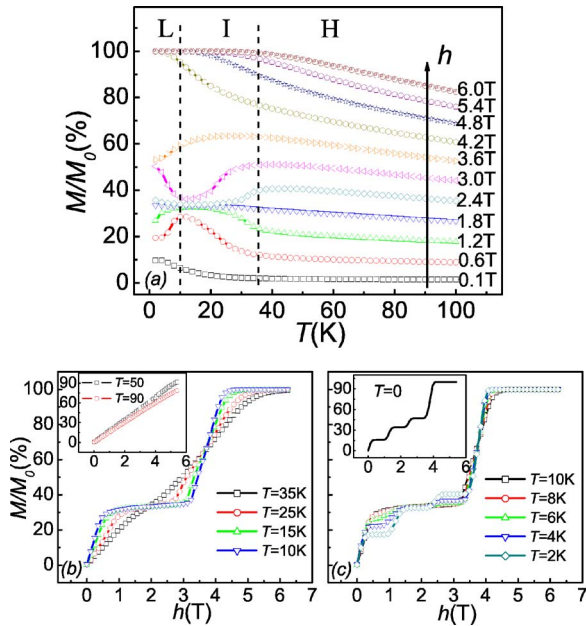


FIG. 1. (Color online) (a) Curves of the magnetization (M/M_0) as functions of T for different h . L , I , and H represent the low T range, intermediate T range, and high T range, respectively; (b) and (c) M/M_0 as functions of h in the intermediate T range and the low T range, respectively. The inset in (b) presents the $M(h)$ curve in the high T range and the insert of (c) gives that at $T=0$.

of M to increasing h is equidistant, i.e., the system shows paramagnetic behavior. As for regime I ($\sim 10 \text{ K} < T < \sim 35 \text{ K}$) M over the whole h range ($0-6.0 \text{ T}$) tends to merge into two different values upon different h , i.e., $M \rightarrow M_0/3$ as $0 < h < 3.6 \text{ T}$ and $M \rightarrow M_0$ as $h > 3.6 \text{ T}$, indicating wide $M_0/3$ plateau. Similarly, in regime L , M tends to merge into four different values upon different h , indicating the multistep behaviors.

In order to understand $M(T)$ curves in Fig. 1(a) more clearly, we replot the simulated M as a function of h at several temperatures in Figs. 1(b) and 1(c). The paramagnetic behavior as shown in regime H of Fig. 1(a) is confirmed in the inset of Fig. 1(b) where M increases linearly with h . In the intermediate T range (regime I) with $10 \text{ K} < T < 35 \text{ K}$, the appearance of the $M_0/3$ plateau at $h < 3.6 \text{ T}$, as shown in Fig. 1(b), is confirmed. As for the low- T range where $T < 10 \text{ K}$ (regime L), the $M_0/3$ plateau decomposes into three substeps, as shown in Fig. 1(c) where the multistep $M(h)$ at $T=0$ is shown as an inset. It is mentioned here that the three substeps are equidistant with the identical width of about $h_{int} \approx 1.2 \text{ T}$, namely the step jump occurs at $h_{S1} \approx 1.2 \text{ T}$, $h_{S2} \approx 2.4 \text{ T}$ and $h_c \approx 3.6 \text{ T}$, although their height is somehow T dependent. These simulated results quantitatively reproduce the steplike magnetic behaviors of $\text{Ca}_3\text{Co}_2\text{O}_6$ compound over the whole T range, as observed in experiments, even if the fluctuations of spin interactions inside the spin chains are ignored.

C. Spin configuration

It would be interesting to establish the relationship between these peculiar multistep behaviors at low T and the

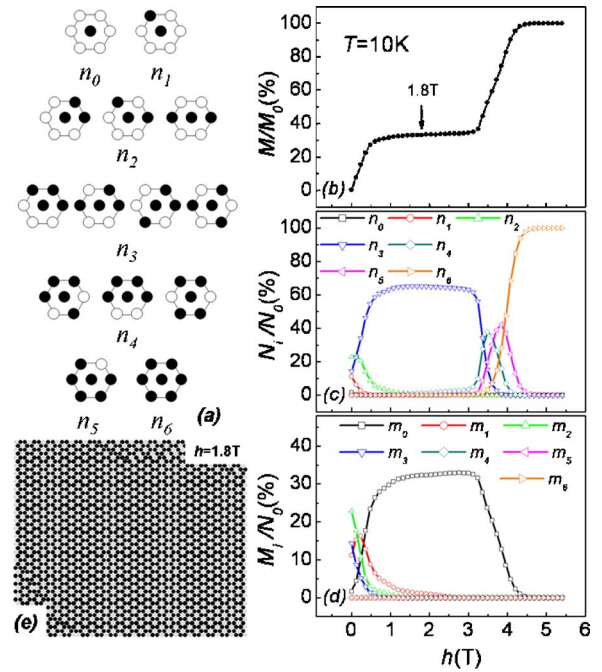


FIG. 2. (Color online) (a) Schematic of the pattern categories: n_0-n_6 , composed of a spin and its six nearest-neighbors; (b) M/M_0 as a function of h at $T=10 \text{ K}$; (c) and (d) h dependence of the NNPC when $T=10 \text{ K}$; (e) 50×50 spin snapshot of the triangular lattice for $h=1.8 \text{ T}$, $T=10 \text{ K}$.

in-plane spin configurations, which was not addressed earlier.²⁸ This relationship is definitely informative for understanding these behaviors in a quantitative sense. The spin configurations at $T=10 \text{ K}$ and 2 K are discussed as examples here. We focus on the nearest-neighboring pattern-count (NNPC) scheme and the spin snapshots to illustrate the spin configurations.

The NNPC scheme means that a spin is categorized by the spin alignments of it and its nearest neighbors (in shorts terminated as “spin pattern” hereafter). There are in total 14 categories of spin patterns. If the orientations of a spin and its x nearest neighbors are all upward, the spin is classified into the category of n_x . In Fig. 2(a) are shown the schematic of these categories: n_0-n_6 , respectively. The black solid circles represent up-spins and the white ones denote down spins. Analogously the other seven categories, m_0-m_6 , are defined as those if a spin and its x nearest neighbors have downward spin orientation, marked as m_x . A scanning of every spin on the whole lattice evaluates the relative amounts (N_i and M_i) of the 14 categories, respectively, normalized by the total number of spins (N_0).

At $T=10 \text{ K}$ (similar at $10 \text{ K} < T < 35 \text{ K}$), the simulated $M(h)$ curve exhibits two plateaus, i.e., M rapidly reaches the first plateau ($\sim M_0/3$) with increasing h from zero, and then switches up to M_0 above $h_c \approx 3.6 \text{ T}$, as shown in Fig. 2(b). The NNPC is shown in Figs. 2(c) and 2(d). It is seen that in corresponding to the $M_0/3$ plateau, two kinds of spin patterns dominate the lattice: about $1/3$ chain spins have pattern m_0 and the other $2/3$ possess pattern n_3 , i.e., the lattice spin configuration consists of

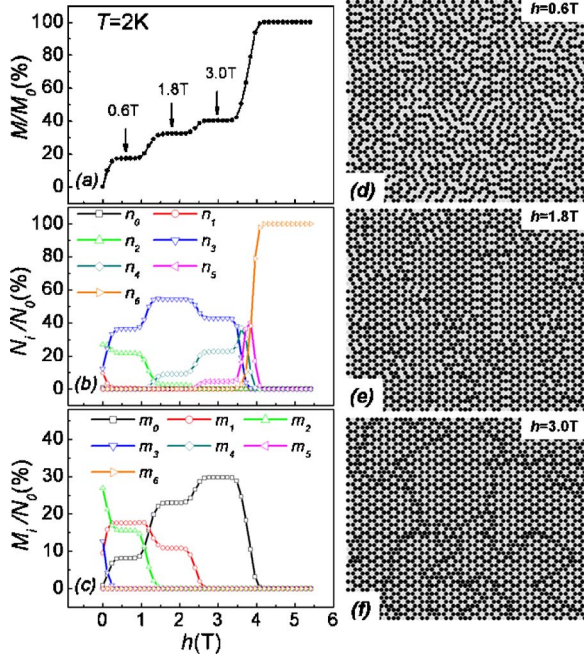


FIG. 3. (Color online) (a) M/M_0 as a function of h at $T=2$ K; (b) and (c) h dependence of the NNPC when $T=2$ K; (d)–(f) 50×50 spin snapshots of the triangular lattice at $T=2$ K for $h=0.6$, 1.8, and 3.0 T, respectively.

$$\frac{2}{3}n_3 + \frac{1}{3}m_0.$$

The height of the plateau is then

$$\left(\frac{2}{3} - \frac{1}{3}\right)M_0 = \frac{1}{3}M_0.$$

Part of the spin snapshot obtained from simulation is presented in Fig. 2(e) at $h=1.8$ T, where the black and gray white circles represent spin up and spin down, respectively. The spin configuration over the whole is homogeneous, showing very regular ferrimagnetic structure consisting of spin patterns n_3 and m_0 . As $h > h_c = 3.6$ T, $M = M_0$ and the spin configuration consists of pattern n_6 only, i.e., the full FM state.

At $T=2$ K (similar at $T < 10$ K), the $M(h)$ curve shows typical four steps: i.e., three substeps occurring at about regular field interval $h_{int} \approx 1.2$ T, namely $h_{S1} \approx 1.2$ T and $h_{S2} \approx 2.4$ T, and the M_0 plateau at $h > h_c \approx 3.6$ T, as presented in Fig. 3(a). This stepwise $M(h)$ curve can be comprehended through the NNPC analysis. As shown in Figs. 3(b) and 3(c), the NNPC as a function of h also shows a stepwise change. Except the last jump, the three substeps are attributed to different combinations of spin patterns, leading to the different heights of the substeps. The first substep below $h=1.2$ T corresponds to the pattern combination

$$n_1 \times 0.4\% + n_2 \times 21.9\% + n_3 \times 36.4\% + m_0 \times 8.1\% \\ + m_1 \times 17.6\% + m_2 \times 15.6\%,$$

resulting in the corresponding step height

$$0.4\% + 21.9\% + 36.4\% - 8.1\% - 17.6\% - 15.6\% \\ = 17.4\% (M_0).$$

The second substep between $h=1.2$ T and 2.4 T is due to the combination

$$n_2 \times 2.6\% + n_3 \times 54.5\% + n_4 \times 9.1\% + m_0 \times 23.0\% \\ + m_1 \times 10.8\%.$$

The corresponding value of M on this substep is

$$2.6\% + 54.5\% + 9.1\% - 23.0\% - 10.8\% = 32.4\% (M_0).$$

The third substep between $h=2.4$ T–3.6 T results from

$$n_3 \times 42.8\% + n_4 \times 22.7\% + n_5 \times 4.7\% + m_0 \times 29.8\%,$$

generating the step height of

$$42.8\% + 22.7\% + 4.7\% - 29.8\% = 40.4\% (M_0).$$

The partial snapshots of the three spin configurations are presented in Figs. 3(d)–3(f), respectively. It is seen that the spin configurations corresponding to the three substeps are inhomogeneous, an essential feature of the spin configuration at low T upon a field not higher than 3.6 T.

The analysis of the spin configurations illustrates that the substeps at $h < 3.6$ T are more or less associated with the long-range ferrimagnetic correlation even at $T=2$ K, though the ferrimagnetism is weaker as T is lower, which was evidenced by neutron diffraction experimental data.²⁷ However, besides the long-range ferrimagnetic ordering, other local spin-ordered areas associated with the substeps are identified. At $h=0.6$ T, one observes some localized FM short stripes with alternative up-spin/down-spin alignment [Fig. 3(d)]. As $h=1.8$ T, the ferrimagnetically ordered areas aggrandize and expand, with a small amount of irregular spin regions [Fig. 3(e)]. At $h=3$ T, these small irregular regions connect with each other, forming the boundaries separating the large-scale ferrimagnetically ordered regions [Fig. 3(f)]. The above analysis allows us to conclude that the substeps observed at low T and not very high field ($h < 3.6$ T) are ascribed to the inhomogeneous spin configurations, while the $M_0/3$ plateau in the intermediate T range is attributed to the homogeneous ferrimagnetic ordering. The coexistence of different spin patterns and thus the inhomogeneous configuration results in this multistep behavior of $M(h)$ at low T .

D. M - h hysteresis

As revealed experimentally in $\text{Ca}_3\text{Co}_2\text{O}_6$, at $T < 10$ K the measured M - h dependence upon the field increasing (FI) and then field decreasing (FD) cycle is hysteretic under steady-state conditions,^{13,14} while no hysteresis can be observed at a relatively high T above 10 K. This hysteretic feature is also reproduced in our simulation. As shown in the insert of Fig. 4(a), no hysteresis is identified at $T=20$ K and above. As T is reduced down to 10 K, a weak hysteresis appears, as shown in Fig. 4(a) where the hysteretic feature is remarkable around $h=0$ and near $h_c=3.6$ T. With further descending of T the hysteresis becomes more significant and spreads over the whole h range below h_c , as shown in Fig. 4(b) for $T=2$ K.

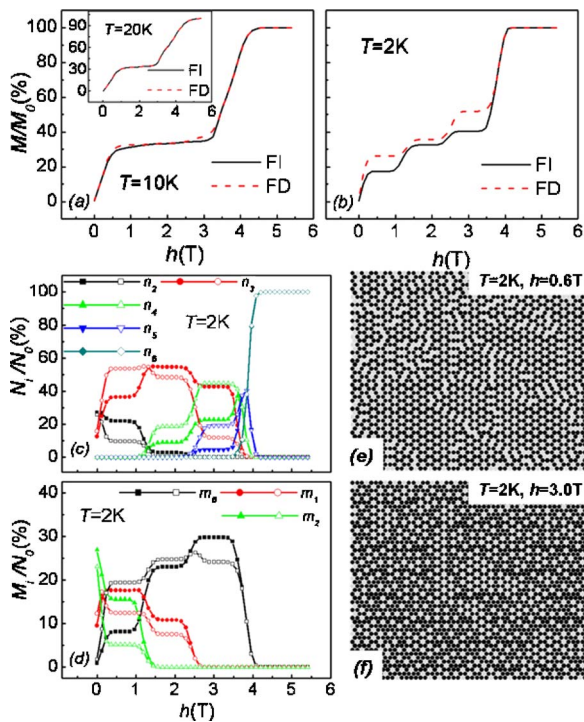


FIG. 4. (Color online) M/M_0 as functions of h with h increasing (FI) and h decreasing (FD), respectively, at (a) 10 K and (b) 2 K, the inset in (a) presents the FI and FD curves at 20 K; (c) and (d) h dependence of the NNPC when $T=2$ K, the FI curves are denoted by solid symbols and FD curves are represented by corresponding open ones; (e), (f) 50×50 spin snapshots of the triangular lattice for $h=0.6$ T and $h=3.0$ T, respectively on the FD branch when $T=2$ K.

These results coincide with available experimental data. The quantitative deviation between the simulation and experiments seems to occur at very low T where the simulated hysteresis is not as significant as the experimentally identified one, probably due to the complexity of real materials that can not be considered in our simulation.

This hysteretic feature at low- T range obviously originates from the inhomogeneous spin frustration states. The corresponding spin configurations are demonstrated by the NNPC as a function of h shown in Figs. 4(c) and 4(d), where the solid dots represent the field dependences during the FI sequence and the open dots are for the FD sequence. The hysteretic behaviors become quite clear. It is seen that the evolution of the spin configuration is path-related. For instance, we look at the h range between 2.4 T and 3.6 T. For the FD sequence the lattice starts from a fully spin-polarized state, and then patterns n_4 and n_5 dominate in the lattice, while for the FI sequence the lattice starts from a ferrimagnetic state and prefers pattern n_3 . We present the spin snapshots taken at $h=0.6$ T and 3.0 T during the FD sequence, respectively, in Figs. 4(e) and 4(f), noting that Figs. 3(d) and 3(f) are the spin snapshots taken at $h=0.6$ T and 3.0 T during the FI sequence. Comparing Figs. 4(e) and 4(f) with Figs. 3(d) and 3(f), one observes that the lattice at $h=3.0$ T during the FD sequence contains much more upward spins than that at $h=3.0$ T during the FI sequence, while the configuration at $h=0.6$ T during the FD sequence prefers the larger-scale fer-

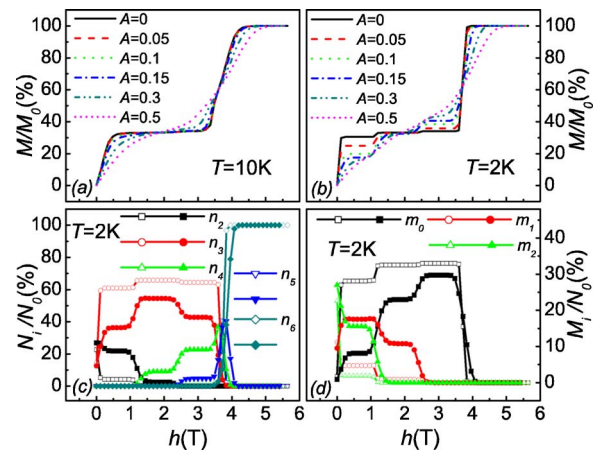


FIG. 5. (Color online) M/M_0 as functions of h for different A at (a) 10 K and (b) 2 K; (c) and (d) h dependence of the NNPC when $T=2$ K. The curves with $A=0$ are denoted by open symbols and those with $A=0.15$ are represented by corresponding solid ones.

rimagnetically ordered regions than that at $h=0.6$ T during the FI sequence.

The path-related configurations indicate that the spin frustration leads to the different metastable states associated with the FI and FD sequences of the hysteresis. In this system the AFM interchain coupling and the triangular lattice introduce magnetic frustration. This geometrical frustration produces a high degeneracy of states, corresponding to multiple energy minimal. Similar to the spin glass, these energy minimal, namely the ground state and metastable states, are very close from one another in energy. At low temperature, during the FI and FD sequences the spin configurations are frozen into different metastable states which are very steady from the viewpoint of dynamics. Therefore the evolution of the spin configuration is path-related, and consequently the hysteresis loop appears.

E. Effect of random exchange interaction

For real materials, in particular for complicated oxides such as the $\text{Ca}_3\text{Co}_2\text{O}_6$ compound studied here, localized defects and nonstoichiometry often results in the spatial fluctuations of the spin interactions. As an effective approach, such fluctuations are usually treated as random fields applied to the lattice. In our simulation, random exchange interaction, as one kind of random field, is taken into account to understand the role of the spatial fluctuations. Figures 5(a) and 5(b) show the simulated $M(h)$ under different random exchanges (A) at $T=10$ K and 2 K, respectively. At $T=10$ K, the system with $A=0$ exhibits the perfect $M_0/3$ plateau. The increasing A seems to melt the plateau gradually and a gradual growth of M with increasing h is established when A is large enough ($A=0.5$). Similar behaviors are observed for the substeps at low T . At $T=2$ K, the M gaps between neighboring steps is very small in case of $A=0$. However, a small A can enhance these gaps greatly, though the step ends are smoothed down either. These substeps may be eventually smeared out if the random exchange is very large ($A=0.5$).

The effects of parameter A on the magnetization $M(h)$ can be explained by the NNPC obtained at $A=0$ (open dots) and 0.15 (solid dots), as presented in Figs. 5(c) and 5(d) at $T=2$ K. When $A=0$, the ferrimagnetic ordering consisting of n_3 and m_0 is dominant in the large h range below h_c . However, as $A=0.15$, the random term enhances the fluctuations of the spin alignment, resulting in the local disordering of the ferrimagnetic configuration and thus appearance of other local spin patterns, i.e., inhomogeneity appears. The coexistence of these inhomogeneous regions leads to easy generation of the obvious substeps in the low T range. At $A=0.5$, the three substeps are almost smeared out due to the enhanced disordering effect. It is noted that the random exchange has an important effect on the heights and sharpness of those substeps, but the $h_{int} \approx 1.2$ T equidistant distribution of steps remains unaltered. The experiment on the effect of doping in $\text{Ca}_3\text{Co}_2\text{O}_6$ shows similar results.¹⁹

F. Influence of the next-nearest neighboring interaction J_{nn}

For the interesting magnetic behavior of triangular spin-chain compounds, besides the nearest-neighboring interaction, longer-range interactions are speculated and discussed in previous investigations.^{15,29} In the pioneer work,²⁹ the triangular Ising lattice with the AFM nearest-neighboring interaction and the FM next-nearest neighboring interaction was used to study the partially disordered antiferromagnetic (PDA) state first observed in CsCoCl_3 . In the present work, we also investigate the effect of the FM next-nearest neighboring interaction (J_{nn}). The Hamiltonian is given by

$$H = - \sum_{[m,n]} (J + J\Delta_{m,n}) S_m^e S_n^e - J_{nn} \sum_{[m,k]} S_m^e S_k^e - h\mu_{BG} \sum_m S_m^e, \quad (3)$$

where $[m,k]$ denotes the summation over all the next-nearest neighboring pairs, and other symbols were well defined above.

Figures 6(a) and 6(b) present the simulated M as functions of h for different J_{nn} at 10 K and 2 K. It is seen that at $T=10$ K the jumps of M with increasing h from zero to $M_0/3$ and then to M_0 becomes sharper with increasing J_{nn} . At $T=2$ K, the height difference between these substeps decreases with increasing J_{nn} , while $h_{int} \approx 1.2$ T equidistant step width seems essentially unchanged. The effect of J_{nn} on the spin configuration can be found in the NNPC shown in Figs. 6(c) and 6(d) at $T=2$ K. Comparing with the case of $J_{nn}=0$, in the case of $J_{nn}=0.05|J|$ patterns n_3 and m_0 are enhanced and the other patterns are suppressed. Therefore, it can be argued that the next-nearest neighboring FM interaction enhances the ferrimagnetic ordering favoring the $M_0/3$ plateau, a quite reasonable result. In fact, for the ferrimagnetic ordering, the next-nearest neighboring spin pairs are aligned in the FM order.

The simulations described above allow us to argue that the inhomogeneous spin configuration as deviating from the ferrimagnetic ordering upon applied magnetic field is the intrinsic origin for the substep formation. The hysteresis, the random exchange interaction, and the next-nearest neighboring FM interaction all can modulate the inhomogeneity of

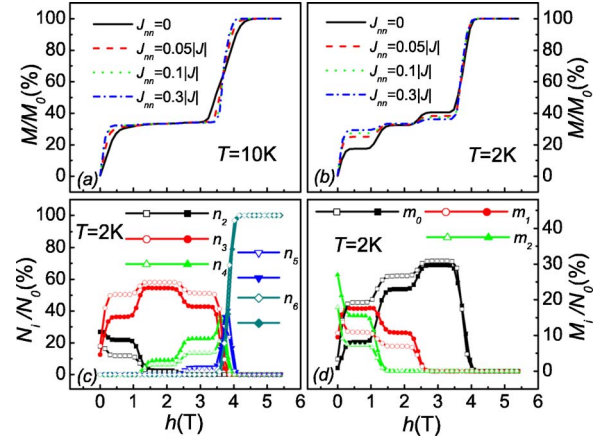


FIG. 6. (Color online) M/M_0 as functions of h for different J_{nn} at (a) 10 K and (b) 2 K. (c) and (d) h dependence of the NNPC when $T=2$ K. The curves with $J_{nn}=0.05|J|$ are denoted by open symbols and those with $J_{nn}=0$ are represented by corresponding solid ones.

the spin configuration, and consequently influence the step-wise magnetic behaviors. However, the 1.2 T equidistant distribution of the substeps, as another intrinsic character, remains essentially unchanged. These results are essentially consistent with experimental observations.

III. MONTE CARLO SIMULATION ON 3D MODEL

A. 3D Ising model

In order to testify the 2D simulation as presented above, we also perform extensive simulation on the 3D model, in particular on the magnetic behavior inside the chains. Considering the 3D anisotropic spatial arrangement and ignoring the phase difference between neighboring chains in $\text{Ca}_3\text{Co}_2\text{O}_6$, we may assume that the Co^{3+} ions are coplanar and then the lattice structure is composed of triangular 2D lattices stacked along the c axis. The spin chain is along the c axis and the intrachain coupling is FM type, namely $J_{intra} > 0$. The interchain coupling (J_{inter}) is AFM type, namely $J_{inter} < 0$. The system Hamiltonian is then expressed as

$$H = - \sum_{[m,l]} J_{intra} S_m S_l - \sum_{[m,n]} J_{inter} S_m S_n - h\mu_{BG} \sum_m S_m, \quad (4)$$

where $[m,l]$ denotes the summation over all the nearest-neighboring pairs in the chains; $[m,n]$ means the summation over all the nearest-neighboring pairs in the ab plane; S_m is the moment of a lattice spin. It was revealed that the crystalline electric field splits the energy level of Co^{3+} ions into the high-spin ($S=2$) and low-spin ($S=0$) states.^{13,22,25} Only the ions of high-spin ($S=2$) contribute to the magnetic properties, so $S_m = \pm 2$ is chosen in the present simulation. The values of other parameters for the simulation are shown in Table I. Similar to the 2D simulation in Sec. II, the values of J_{intra} and J_{inter} are judged from a quantitative comparison between the simulated results and experimental data. The procedure of simulation also resembles an earlier one for the 2D simulation and an $L \times L \times L$ ($L=40$) lattice is employed.

In fact, the critical issue for the 3D simulation is to confirm the argument that the relaxation of spins along the chains is much faster than that for the interchain spin relaxation in the ab plane. If this argument is true, it may be reasonably convinced that each chain in the 3D lattice can be treated as a giant spin, and consequently the 3D lattice is simplified into the 2D triangle lattice with giant spin moment. Generally, the relaxation time τ for a spin flipping from one state to the other has the form $\tau = \tau_0 \exp(\Delta H/T)$, where ΔH is the energy difference of H before and after the spin flip.³⁰ The prefactor τ_0 depends on the interaction J for a spin pair in an exponential form e^{-aJ} . Therefore, a small increase of J will reduce τ_0 very greatly, and sequentially reduce τ . When the FM interaction in the chains is strong, τ is so short that the intrachain spin flips proceed in an avalanche manner. In other words, due to the fact that for the intrachain event, prefactor τ_0 depends on the interaction J , the time unit for Monte Carlo event is different from that for the spin flip event in the ab plane.

Therefore, in our 3D simulation, the single spin flip is improved to include the synchronous flip of several neighboring spins. The flip probabilities of one spin or several neighboring spins are calculated respectively according to the Metropolis algorithm, based on the change of energy resulting from the spin flips. Then the stochastic flipping of spins is approved based on these flip probabilities. Consequently the mechanism of spin flipping includes flipping of several neighboring spins. For an example, if the flipping of x neighboring spins leads to more reduction of energy, its occurrence has a larger probability.

B. Stepwise behavior

The simulation results of the 3D model at different temperatures, as demonstrated in Fig. 7(a), show magnetic behaviors similar to the results of the 2D model, which testifies the appropriateness of the approximation used in 2D simulation. As shown in Fig. 7(a), when T is above 25 K, M as a function of h shows the paramagnetic behavior. In the T range from 25 K to 10 K, the wide $M_0/3$ plateau appears gradually with decreasing T . As T is below 10 K, three sub-steps emerge at regular intervals of $h_{int} \approx 1.2$ T below $h_c \approx 3.6$ T, and the $M(h)$ curve at $T=2$ K is illustrated in the insert of Fig. 7(a). Though the phase difference between neighboring chains is ignored, the results of 3D simulation are also in agreement with experimental data, which proves that the interchain AFM interaction plays an important role in the steplike magnetic behavior, regardless of the detailed structure of the spin-chains.

C. Intrachain behavior

In order to understand the magnetic behavior of the spin-chains in a more detailed way, we investigate the dynamics of the intrachain spin flipping and spin snapshots under zero-field condition. Because several spins in the same chain can flip together, the number of these spins which flip synchronously in a chain is an important parameter to investigate the intrachain dynamics of spin flipping. In our simulation the average value of these spin numbers, namely the average

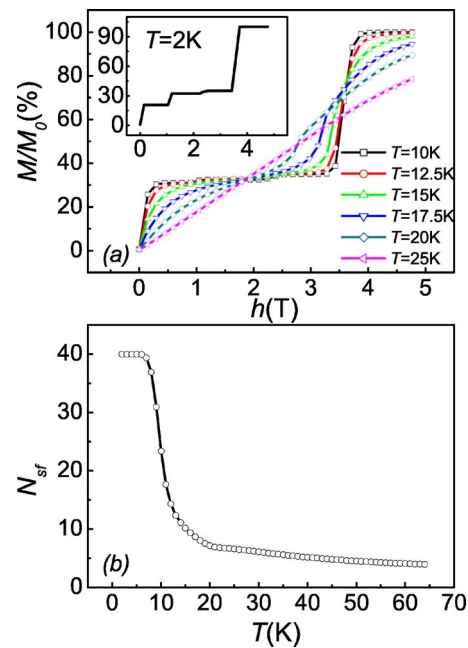


FIG. 7. (Color online) (a) M/M_0 as functions of h at different T . The insert of (a) gives $M(h)$ curve at $T=2$ K. (b) The average spin flipping number (N_{sf}) as a function of T with $h=0$.

spin flipping number (N_{sf}), is calculated as a function of T at $h=0$. In detail it can be calculated as follows: at a certain temperature, every time when one or more than one spins flip, the number of flipping spins is summed up and at last the sum is divided by the total time of flips. That is, if the number of flipping spins for one time is denoted as a_i , and the total time of spin flips is represented as F , then

$$N_{sf} = \sum_{i=1}^F a_i / F.$$

Parameter N_{sf} as a function of T at $h=0$ is presented in Fig. 7(b). It is seen that at low T ($T < 10$ K), all spins in one chain prefer to flip synchronously. When T increases up to about 10 K, a great fall of N_{sf} is observed. Further increasing of T up to 25 K and above, N_{sf} decays gradually and the spin flip inside one chain becomes an individual spin event. Accordingly, the sectional snapshots at $h=0$ are demonstrated in Fig. 8 where the 2D snapshots along the c axis are presented in the left column and those perpendicular to the c axis (i.e., ab sectioned) are correspondingly illustrated in the right column, with $T=5, 15, 50$ K from top. It is observed that at low $T \sim 5$ K, all the spins in one chain align in the same direction [Fig. 8(a)]. The spin configuration in the ab plane shows a partially disordered state, from which many local PDA areas can be identified [Fig. 8(b)]. When T is around 15 K where $N_{sf} \sim 10$, the snapshot shown in Fig. 8(c) indicates that for some chains all spins aligned in the same direction, while they do no longer for the other chains. The spin configuration in the ab plane is inhomogeneous and consists of small ferromagnetic regions and PDA areas [Fig. 8(d)]. At $T=50$ K, as shown in Figs. 8(e) and 8(f), only short-ranged FM clusters

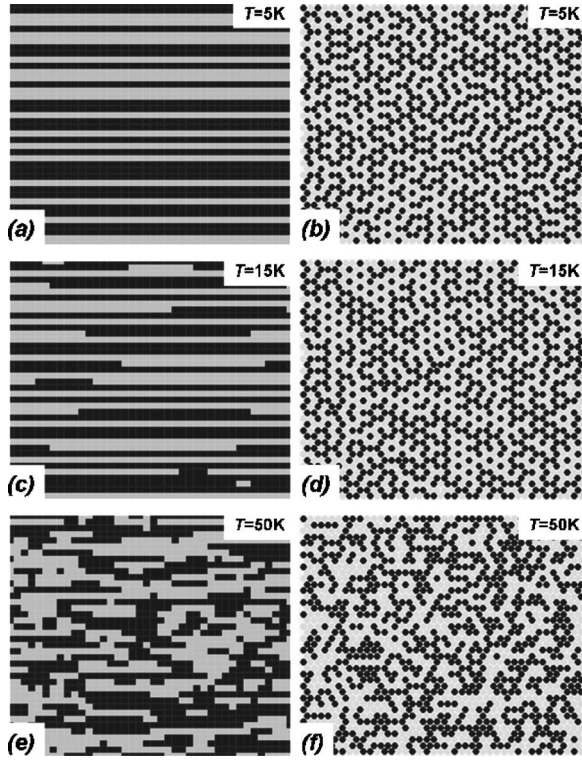


FIG. 8. (a), (c), (e) Sectional snapshots along c axis and (b), (d), (f) sectional snapshots perpendicular to c axis without external magnetic field at different T (from the top down, $T=5, 15$, and 50 K).

along the chains are observed, and the ab -planar spin configuration becomes paramagnetic.

From the above 3D simulation, it is indicated that at low T , all spins in each chain preserve the same orientation and flip together, which confirms our argument in the 2D model that a chain can be regarded as a rigid giant spin. When T is high, this approximation will not be appropriate, but has no influence on the conclusion derived from the 2D simulations.

D. Equidistant distribution of magnetization steps

As presented above, the complex magnetic behaviors as observed in $\text{Ca}_3\text{Co}_2\text{O}_6$ compound can be reproduced quantitatively in our simulations on both 2D and 3D Ising-like models. It is indicated that the AFM interchain coupling and the triangular lattice introduce magnetic frustration, which insure the stability of the magnetization steps. Therefore, the interchain AFM interaction plays an important role in forging the stepwise behavior of magnetization.

An important character of the multistep behavior is the equidistant distribution of steps. In our model it is due to the competition of the exchange interaction term and the magnetic field term in the Hamiltonian. In the 2D Hamiltonian [Eq. (1)], as the first-order approximation, the Hamiltonian for a spin S_m^e is $H_m = -JS_m^e \sum S_n^e - h\mu_B g S_m^e$, where the first item $-JS_m^e \sum S_n^e$ represents the interaction energy and the second one $-h\mu_B g S_m^e$ is the magnetic Zeeman energy. The two energy terms compete with each other, namely $J \sum S_n^e$ vs $h\mu_B g$. Here $\sum S_n^e$ is the summary of the six nearest-

neighboring spins. When one of the six nearest-neighboring spins flips, for instance, changes from S to $-S$. The change of $\sum S_n^e$ is $S - (-S) = 2S$. So $2JS$ is the unit for change of $J \sum S_n^e$, which corresponds to the interval of the critical spin-flip fields $h_{\text{int}} = 2S^e J / (g\mu_B) \sim 1.2$ T.

For the 3D model, our simulation presents that all spins in one chain flip together at low T . Therefore, the first term in Eq. (4) (including J_{intra}) hardly contributes to h_{int} . Similar to the 2D case, in 3D model $h_{\text{int}} = 2|S|J_{\text{inter}} / (g\mu_B) \sim 1.2$ T, i.e., the critical fields for spin flip are $h_{S1} = 1h_{\text{int}} \approx 1.2$ T, $h_{S2} = 2h_{\text{int}} \approx 2.4$ T, $h_c = 3h_{\text{int}} \approx 3.6$ T, resulting in the equidistant distribution of magnetization steps. Our simulation indicates that the $h_{\text{int}} \approx 1.2$ T equidistant distribution of the steps is an intrinsic character resulting from AFM interchain interaction. This character cannot be easily altered by other factors like random exchange term and next-nearest neighboring FM interaction, which is consistent with previous experimental results.^{13,19}

IV. MEAN FIELD APPROXIMATION

In this section, we employ the mean field approach to study the magnetic behavior of the triangular lattice. Although this approach is less precise, it allows us to check the present simulated data. The main idea of the present approach remains similar to the 2D Ising-like model discussed in Sec. II. A loop-wise scheme (LWS) (Ref. 31) is used. As shown in Fig. 2 of Ref. 31, the triangular lattice is partitioned into two interpenetrated sub-lattices which are composed of plaquettes A and B , respectively. For A plaquette, we label the relative values of the three fluctuating spins as S_1, S_2, S_3 , and for B plaquette M_1, M_2, M_3 are introduced as the relative values of the three magnetizations. The Hamiltonian of plaquette A then writes

$$H = -J(S^e)^2(S_1S_2 + S_2S_3 + S_3S_1) - 2J(S^e)^2[S_1(M_2 + M_3) + S_2(M_3 + M_1) + S_3(M_1 + M_2)] - hS^e(S_1 + S_2 + S_3), \quad (5)$$

where J is the interchain AFM interaction ($J < 0$); S^e is the effective value of a spin chain. Considering the spatial fluctuation of the system, a random exchange interaction term $\Delta_{m,n}$ as given in Eq. (2) is taken into account. Then J is replaced by $J_{m,n}$, namely

$$J_{m,n} = J + J\Delta_{m,n}. \quad (6)$$

The three thermal averages of S_1, S_2, S_3 are given by

$$\langle S_i \rangle = \frac{1}{Z} \sum_{S_j^e = \pm 1} S_i \exp(-\beta H), \quad (7)$$

where $\beta \equiv 1/(k_B T)$, $i = 1, 2, 3$, and Z is the partition function taking the form

$$Z = \sum_{S_i^e = \pm 1} \exp(-\beta H). \quad (8)$$

The associated three self-consistent equations are written as

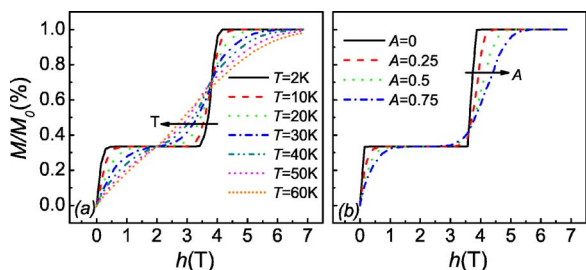


FIG. 9. (Color online) Curves of M/M_0 as functions of h (a) with $A=0.15$ for different T and (b) for different A at $T=2$ K.

$$\langle S_i \rangle = M_i. \quad (9)$$

The self-consistent equations are solved using the parameters given in Table I. According to the previous investigation,^{13,14} PDA phase is suggested in low field, so $S_1=1$, $S_2=-1$, and $S_3=0$ are chosen as the initial states. The calculation is done in an iteration way until a well-defined convergence state. Then the magnetization is calculated as below

$$M = (M_1 + M_2 + M_3)/3. \quad (10)$$

The h dependences of M at different T are presented in Fig. 9(a). It is seen that the $M_0/3$ plateau at $T=10$ K is similar to our simulation results. With increasing T , the plateau disappears gradually.

Unfortunately, in the mean-field framework the three substeps never appear when T decreases below 10 K. Upon changing of A at $T=2$ K, the calculated $M(h)$ curves are plotted in Fig. 9(b), from which one finds that the random exchange term only smoothes the jumps, but cannot result in additional steps. The reason is not hard to understand. The $M_0/3$ plateau attributes to the homogeneous ferrimagnetic state, which is accessible by the MFA. For the multistep behaviors, our simulations demonstrate that the spin configuration is inhomogeneous and the MFA may not be employed

to predict the inhomogeneous state. Due to too less fluctuating degrees of freedom considered, the simple MFA ignores the condition that many configurations with equal energy coexist. In another word, the multiple steps correspond to the multiple potential wells of the free energy function,³² which cannot be obtained in the MFA.

V. CONCLUSION

In summary, the magnetic properties of a spin-chain system in triangular lattice are extensively investigated using Monte Carlo simulation and mean-field approximation. In Monte Carlo simulation of the 2D Ising-like model, in order to establish the relationship between stepwise behaviors and the spin configurations in the ab plane, the NNPC and spin snapshots are employed to characterize the spin configurations under different conditions. For the simulation of the 3D model, the spin flipping and snapshots in the chains at different temperature are presented to understand the intrachain spin behavior. In addition, a mean-field approximation is employed to study the magnetic properties as a supplement. It is argued that the $M_0/3$ plateau in the intermediate T range corresponds to a homogeneous ferrimagnetic ordering, while the multiple steps in the low T range originate from inhomogeneous spin configurations. These inhomogeneous states in the low T range are sensitive to system fluctuations such as the random exchange term and the FM next-nearest neighboring interaction. However, the 1.2 T equidistant distribution of steps, as an intrinsic character only relating to the spin moment and AFM interchain interaction, preserves unchanged.

ACKNOWLEDGMENTS

The authors thank the Natural Science Foundation of China (50332020, 10021001) and the National Key Projects for Basic Research of China (2002CB613303, 2004CB619004).

*Corresponding author. Email address: liujm@nju.edu.cn

¹M. Oshikawa, M. Yamanaka, and I. Affleck, Phys. Rev. Lett. **78**, 1984 (1997).

²D. C. Cabra, A. Honecker, and P. Pujol, Phys. Rev. Lett. **79**, 5126 (1997).

³T. Vekua, D. C. Cabra, A. Dobry, C. Gazza, and D. Poilblanc, Phys. Rev. Lett. **96**, 117205 (2006).

⁴S. T. Bramwell and M. P. Gingras, Science **294**, 1495 (2001).

⁵J. Wu, H. Zheng, J. F. Mitchell, and C. Leighton, Phys. Rev. B **73**, 020404(R) (2006).

⁶M. F. Collins and O. A. Petrenko, Can. J. Phys. **75**, 605 (1997).

⁷S. Rayaprol, K. Sengupta, and E. V. Sampathkumaran, Solid State Commun. **128**, 79 (2003).

⁸R. Vidya, P. Ravindran, H. Fjellvag, A. Kjekshus, and O. Eriksson, Phys. Rev. Lett. **91**, 186404 (2003).

⁹E. V. Sampathkumaran and A. Niazi, Phys. Rev. B **65**, 180401(R) (2002).

¹⁰V. Hardy, M. R. Lees, A. Maignan, S. Hébert, D. Flahaut, C. Martin, and D. M. Paul, J. Phys.: Condens. Matter **15**, 5737 (2003).

¹¹H. Fjellvag, E. Gulbrandsen, S. Aasland, A. Olsen, and B. C. Hauback, J. Solid State Chem. **124**, 190 (1996).

¹²S. Aasland, H. Fjellvag, and B. Hauback, Solid State Commun. **101**, 187 (1997).

¹³H. Kageyama, K. Yoshimura, K. Kosuge, M. Azuma, M. Takano, H. Mitamura, and T. Goto, J. Phys. Soc. Jpn. **66**, 3996 (1997).

¹⁴H. Kageyama, K. Yoshimura, K. Kosuge, H. Mitamura, and T. Goto, J. Phys. Soc. Jpn. **66**, 1607 (1997).

¹⁵A. Maignan, C. Michel, A. C. Masset, C. Martin, and B. Raveau, Eur. Phys. J. B **15**, 657 (2000).

¹⁶V. Hardy, S. Lambert, M. R. Lees, and D. M. Paul, Phys. Rev. B **68**, 014424 (2003).

¹⁷B. Martínez, V. Laukhin, M. Hernando, J. Fontcuberta, M. Parras, and J. M. González-Calbet, Phys. Rev. B **64**, 012417 (2001).

- ¹⁸B. Raquet, M. N. Baibich, J. M. Broto, H. Rakoto, S. Lambert, and A. Maignan, *Phys. Rev. B* **65**, 104442 (2002).
- ¹⁹D. Flahaut, A. Maignan, S. Hebert, C. Martin, R. Retoux, and V. Hardy, *Phys. Rev. B* **70**, 094418 (2004).
- ²⁰R. Fresard, C. Laschinger, T. Kopp, and V. Eyert, *Phys. Rev. B* **69**, 140405(R) (2004)
- ²¹E. V. Sampathkumaran, N. Fujiwara, S. Rayaprol, P. K. Madhu, and Y. Uwatoko, *Phys. Rev. B* **70**, 014437 (2004).
- ²²O. A. Petrenko, J. Wooldridge, M. R. Lees, P. Manuel, and V. Hardy, *Eur. Phys. J. B* **47**, 79 (2005).
- ²³V. Hardy, M. R. Lees, O. A. Petrenko, D. M. Paul, D. Flahaut, S. Hébert, and A. Maignan, *Phys. Rev. B* **70**, 064424 (2004).
- ²⁴A. Maignan, V. Hardy, S. Hebert, M. Drillon, M. R. Lees, O. Petrenko, D. M. K. Paul, and D. Khomskii, *J. Mater. Chem.* **14**, 1231 (2004).
- ²⁵H. Wu, M. W. Haverkort, Z. Hu, D. I. Khomskii, and L. H. Tjeng, *Phys. Rev. Lett.* **95**, 186401 (2005).
- ²⁶Y. B. Kudasov, *Phys. Rev. Lett.* **96**, 027212 (2006).
- ²⁷H. Kageyama, K. Yoshimura, K. Kosuge, X. Xu, and S. Kawano, *J. Phys. Soc. Jpn.* **67**, 357 (1998).
- ²⁸X. Y. Yao, S. Dong, and J.-M. Liu, *Phys. Rev. B* **73**, 212415 (2006).
- ²⁹M. Mekata, *J. Phys. Soc. Jpn.* **42**, 76 (1977).
- ³⁰C. C. Su, B. Vugmeister, and A. G. Khachatryan, *J. Appl. Phys.* **90**, 6345 (2001); J.-M. Liu, X. Wang, H. L. W. Chan, and C. L. Choy, *Phys. Rev. B* **69**, 094114 (2004).
- ³¹S. Galam and P. V. Koseleff, *Eur. Phys. J. B* **28**, 149 (2002).
- ³²H. Yu, Y. Wang, J. -M. Liu, H. L. W. Chan, and C. L. Choy, *J. Phys.: Condens. Matter* **15**, 8631 (2003).